AD661813

Document D6-60083
September 1967

Some Characteristics of Aqueous Stress Corrosion in Titanium Alloys

D.N. Fager and W.F. Spurr

The BOEING Company
Commercial Airplane Division
Renton, Washington

DEC 4 1967

Sponsored by
Advanced Research Projects Agency
ARPA Order No. 878

Reproduced by the
CLEARINGHOUSE
for Federal Scientific & Technical
Information Springfield Va. 22151

20

Some Characteristics of Aqueous Stress Corrosion in Titanium Alloys

D. N. Fager and W. F. Spurr

Abstract

The influence of microstructural features on the stress corrosion fracture path has been studied in the alloys Ti-8Al-1Mo-1V, Ti-6Al-4V, Ti-4Al-3Mo-1V, Ti-5Al-2.5Sn, and Ti-13V-11Cr-3Al by means of optical microscopy, electron microscopy, and X-ray diffraction. These studies have shown that susceptibility of titanium alloys to aqueous stress corrosion is influenced by crystalline structure of the susceptible phase (bcc or hcp), preferred grain orientation, and relative phase content where one phase is immune. Stress corrosion cracking occurs on or near the {100} planes in the bcc beta phase, but can only occur near the single (0001) plane in the hcp alpha phase. This restriction of cracking in the alpha phase results in a significant influence due to preferred orientation; it also contributes to the influence of stress state on susceptibility in the high-alpha alloys. The apparent lack of correlation between the structures of the phases and their stress corrosion susceptibilities indicates that the basic mechanism is surface-controlled rather than structurally controlled.

The authors are associated with the Commercial Airplane Division of The Boeing Company, Seattle, Washington.

Introduction

Stress corrosion of titanium alloys in chloride environments has been a matter of concern for the past ten years. Before 1965, it was considered a high-temperature problem (hot-salt stress corrosion). In 1965, however, Brown (1) discovered the effect known as aqueous stress corrosion whereby, under special conditions, titanium alloys crack at room temperature in salt water. Further studies revealed that few, if any, of the commercial titanium alloys in one heat-treatment condition or another are immune to this type of stress corrosion.

Brown subjected notched, fatigue-cracked specimens to a bending stress and found that they failed faster and at lower load levels in salt water than in air. Without the notch or fatigue crack, most previous studies had revealed no effect due to salt water. An exception was the 1960 study of Crossley, et al (2), in which two static fatigue tests in salt water were run on the beta (β) alloy Ti-13V-11Cr-3Al. In both tests, the specimens failed at the yield point with slight elongation. Most development work in titanium, however, has been on high-alpha (α) alloys, in which it is difficult (if possible) to obtain an effect due to salt water with unnotched specimens.

Aqueous stress corrosion in titanium alloys is characterized by extremely fast crack growth rates. In a precracked specimen, the average rate may be faster than 50 in./hr compared with average stress-corrosion cracking rates of less than 1 in./hr (3) in other alloy systems (excluding liquid metal embrittlement). Because of this high rate, stress corrosion effects may be seen in specimens dynamically loaded to failure, whereas a static test is normally required.

In this study, metallurgical variables influencing stress corrosion susceptibility were investigated in several commercial titanium alloys. Optical microscopy, electron microscopy, and X-ray diffraction were used to determine the relation between the stress corrosion fracture path and microstructural features.

Experimental Procedure

Table 1 lists the alloys used in this study, along with estimates of the phase contents at conventional annealing temperatures. All but Ti-13V-11Cr-3Al are referred to herein as "high-α" alloys.

Precracked, notched bend specimens were used for most of the testing.[1] The specimens were transverse-longitudinal,[2] except those used in the crack propagation study on Ti-8Al-1Mo-1V. The two specimen configurations were (a) three-point-loaded, Charpy size, and (b) four-point-loaded, 0.480 by 1.5 by 7.5 in. (4). Two specimens of the three-point-loaded configuration were loaded to failure at 300 lb/min to obtain a baseline toughness value. Other specimens were then loaded to various percentages of the baseline value, 3.5% sodium chloride solution was added, and time to failure was recorded. Because the high crack propagation rate usually caused failure within 10 min, the maximum test time was set at 1 hr. The same test procedure was used for the four-point-loaded specimens, except that a 14,500-lb/min loading rate was used to obtain the baseline value and the test time was extended to 6 hr. The data was interpreted by means of a fracture mechanics analysis. Standard formulas (5) were used to convert the load and crack depth values to the stress intensity factor K.

The K value calculated from a baseline specimen is the plane-strain critical stress intensity factor K_{IC}. The sustained-load K values have been designated K_{Ii}, the initial stress intensity value prior to crack extension.

The validity of a K value depends on yield strength, actual fracture toughness level, and specimen geometry (5). The tensile yield

---

[1]Center-cracked panels were used to demonstrate the thickness effect in the high-α alloys. See Ref. 4 for a description of the specimens and test procedure.

[2]The first direction is the grain direction from which the long dimension of the specimen was taken; the second, the direction of crack propagation. (See Fig. 12.)

Table I. Alloy identification.

Alloy	Heat number	Chemistry										% of β (a)
		wt %							ppm			
		Al	Mo	V	Cr	Sn	Fe	C	H	O	N	
Ti-5Al-2.5Sn	301064	6.0	---	---	---	2.2	0.15	---	72	1385	60	5
Ti-8Al-1Mo-1V	291870	7.4	1.2	1.1	---	---	0.05	0.05	63	1310	47	10
Ti-6Al-4V	D4988	6.4	---	3.9	---	---	0.17	0.03	30	1500	180	15
Ti-4Al-3Mo-1V	D9484	4.5	3.3	1.0	---	---	0.10	0.03	60	1100	90	25
Ti-13V-11Cr-3Al	---	3.3	---	13.2	10.3	---	0.15	0.03	102	1080	400	95

[a] Approximation after conventional annealing.

strengths of the specimens tested ranged approximately from 120 to 140 ksi. The large four-point-loaded specimen provides plane-strain fracture toughness values of greater validity and was used where needed to verify results from the smaller specimens. Where the specimen geometry was such that invalidity of toughness values obviously influenced the stress corrosion data, the term "apparent fracture toughness" was used.

Deciding how to measure and compare susceptibility is always a problem in stress corrosion testing. In this study, the obvious method was to compare the sustained-load data in salt water against that in an inert environment. Because of the difficulty in using an inert environment, an air environment was considered a reasonable substitute. It was found, however, that sustained-load air failures occurred below the K_{IC} values in some alloys and not in others. This may be a strain-rate effect, a humidity effect, or general yielding.

With sustained-load air testing ruled out as a general procedure, the method used was to compare the salt-water data against the baseline K_{IC}. All conclusions derived from the tests were substantiated by optical microscopy of the crack paths.

Wherever there was a question of complete immunity, the salt-water sustained-load data was compared against that in air. This was justified on the basis that any effects of salt water should result in a difference between the air and salt-water failure curves regardless of the reason for the decrease in air. Thus the ratio K_{Ii}/K_{IC} or K_{Ii}/K^*_{IC} is plotted as a function of failure time, where K^*_{IC} is the minimum of the sustained-load curve in air.

Results and Discussion

CRACKING CHARACTERISTICS IN HIGH-ALPHA ALLOYS

Figures 1 and 2 show the transgranular fracture paths typical of aqueous stress corrosion in high-α alloys. The brittle fracture mode (cleavage) is shown at A in Fig. 3, along with ductile failure (B) due to unfavorable grain

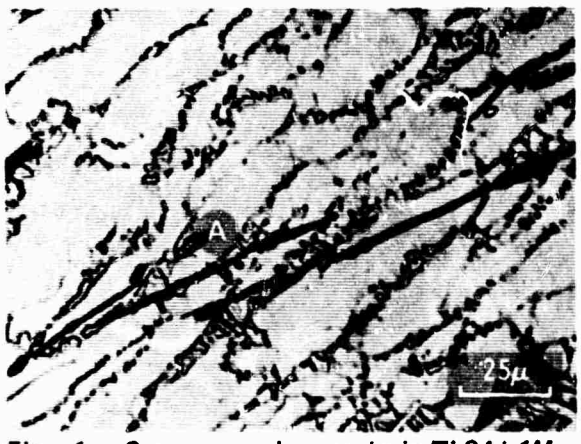

Fig. 1. Stress corrosion cracks in Ti-8Al-1Mo-1V 0.5-in. annealed plate, viewed normal to propagation direction (short transverse view). The β-phase particle at A behaves in a ductile manner.

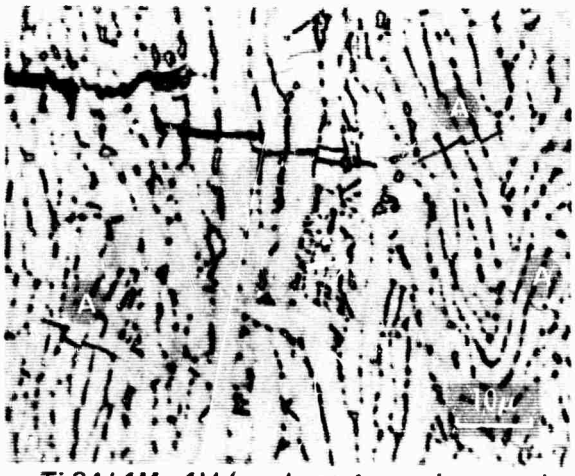

a. Ti-8Al-1Mo-1V (cracks at A remain normal to length of stringers).

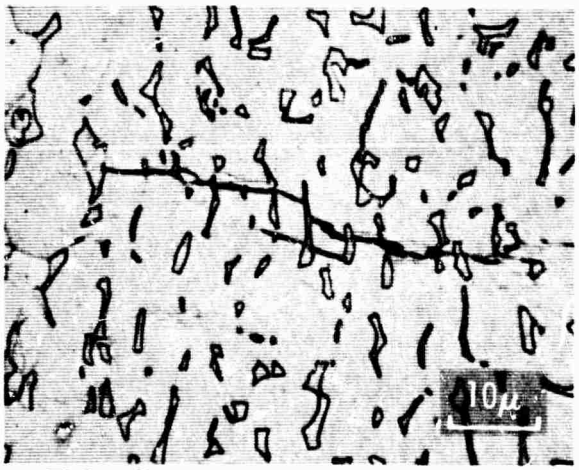

b. Ti-6Al-4V.

c. Ti-4Al-3Mo-1V.

Fig. 2. Stress corrosion cracks in high-α alloys (0.5-in. annealed plate), viewed parallel to propagation direction (longitudinal views).

Fig. 3. Fractograph showing cleavage (A) in the single-phase hexagonal martensite of Ti-5Al-2.5Sn (2000 F/15 min/WQ). Ductile failure occurred at B.

orientation. Since cracks do not generally occur in the β phase of these high-α alloys, this phase appears to be immune to stress corrosion. Figure 1 illustrates this phenomenon in Ti-8Al-1Mo-1V, where the β-phase particle in the fracture path at A extends in a ductile manner instead of cracking. Other cracks in Ti-8Al-1Mo-1V (Fig. 2a), Ti-6Al-4V (Fig. 2b), and Ti-4Al-3Mo-1V (Fig. 2c) show a tendency to be either arrested or diverted by the β phase.

This immunity of the β phase is consistent with the trend of stress corrosion susceptibility with β content in high-α alloys containing molybdenum and vanadium (4,6). Valid comparisons based on β content are difficult to obtain, however, because other variables, such as preferred orientation, can change measured susceptibilities considerably.

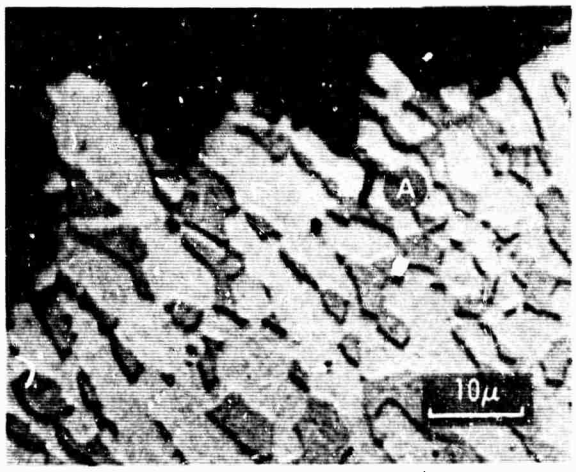

Fig. 4. Stress corrosion crack (A) in α ending at α′ in Ti-8Al-1Mo-1V (1800 F/WQ).

The amount of retained β phase in Ti-8Al-1Mo-1V increases with increasing solution-treating temperature until the martensitic transformation temperature is raised above room temperature. At this point β transforms to martensite upon quenching. Like β, martensite is apparently immune to stress corrosion and inhibits cracks more efficiently as its percentage in the alloy increases. Figures 4 and 5 show examples where cracks occur in the primary α phase but not in either the low-temperature or high-temperature forms of martensite that Blackburn (7) designates α′ and α″. Figure 6 shows the increased stress corrosion resistance of the 1800°F and 1875°F solution-treatment conditions, compared with that of the annealed condition.

The α grains in annealed Ti-8Al-1Mo-1V contain regions of the ordered α phase (8); this was evidenced by superlattice reflections in the electron diffraction patterns. The ordered domains do not remain in the primary α phase when it is quenched from 1800°F or 1875°F. Cracking thus occurs in the α phase with or without the presence of the ordered domains.

When this alloy is heated into the β-phase region and quenched, it is completely transformed to α″ and is immune to stress corrosion. Aging the α″ produces the two-phase α + β structure, rendering the alloy again susceptible (Fig. 7). Figure 8 shows cracks in the acicular grains of the aged α″. The small dark particles are the β precipitate. Crack propagation was difficult because of the small grain size and the difference in orientation between adjacent grains.

The Ti-6Al-4V and Ti-5Al-2.5Sn alloys were also tested in their martensitic conditions; the Ti-6Al-4V martensite, similar to the Ti-8Al-1Mo-1V martensite, was found to be immune, whereas the Ti-5Al-2.5Sn martensite

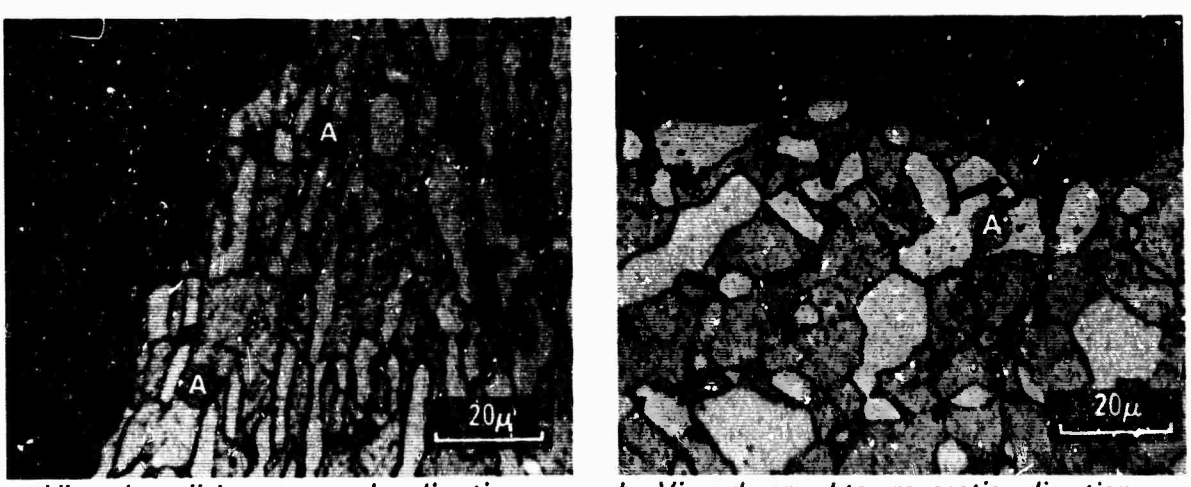

a. Viewed parallel to propagation direction. *b. Viewed normal to propagation direction.*

Fig. 5. Stress corrosion cracks (A) in α inhibited by α″ of Ti-8Al-1Mo-1V (1875 F/WQ).

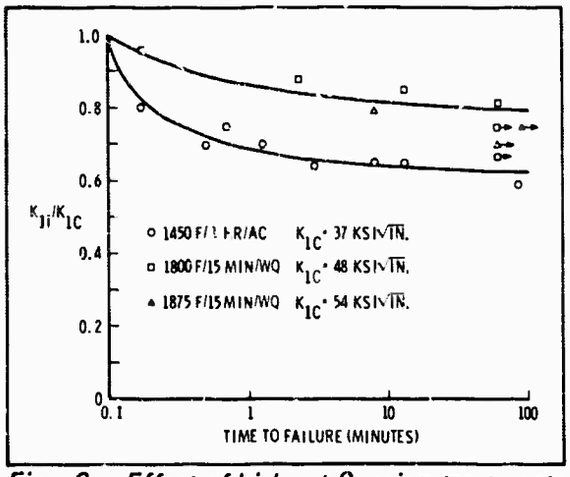

Fig. 6. Effect of high α + β region treatments on Ti-8Al-1Mo-1V stress corrosion susceptibility (three-point-loaded notched bend specimens).

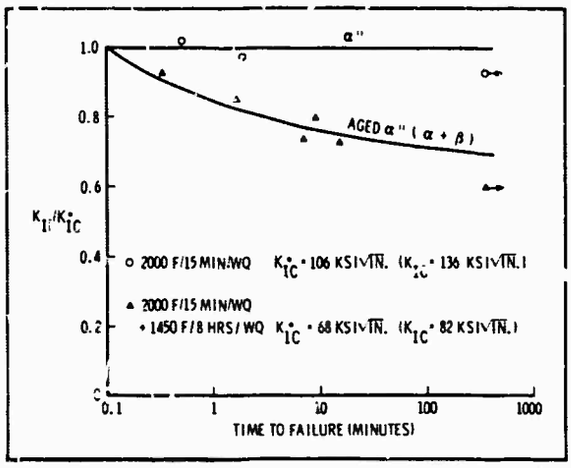

Fig. 7. Stress corrosion susceptibility of α" and aged α" (α+β)– Ti-8Al-1Mo-1V (large four-point-loaded notched bend specimens).

was extremely susceptible (Fig. 9). Figure 10 shows a typical stress corrosion crack in the Ti-5Al-2.5Sn martensite. Cracks were frequently found to extend across many similarly oriented adjacent martensite plates. In areas where more variants of the martensitic transformation appeared, the crack path was less regular.

Grain orientation is a microstructural feature that significantly influences the fracture path. In Fig. 2a, as the direction of α grain elongation changes from one area to

Fig. 8. Stress corrosion cracks in aged α" (α + β) of Ti-8Al-1Mo-1V (2000 F/WQ + 1450 F/8 hr/WQ).

another, the cracks at A remain normal to the length of the elongated grains (stringers). As shown in Fig. 11 (where view A, identical with Fig. 2a, is normal to view B), the cracks are approximately normal to the surface shown in Fig. 2a; this observation was made several times. By using transmission electron microscopy, the basal planes (0001) in 75% of the stringers examined were found to be oriented approximately normal to the length (as shown

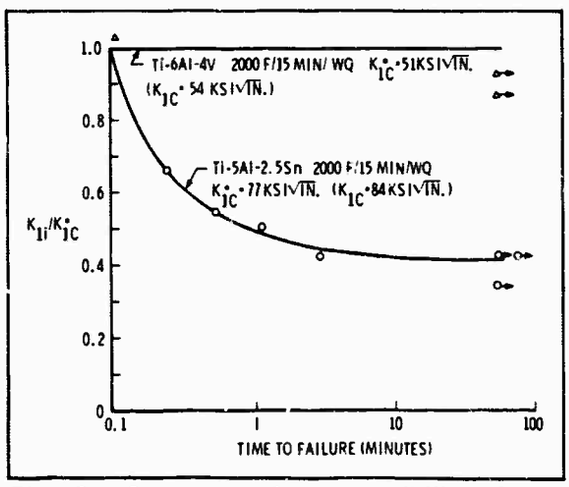

Fig. 9. Stress corrosion susceptibility of Ti-6Al-4V and Ti-5Al-2.5Sn martensites (three-point-loaded notched bend specimens).

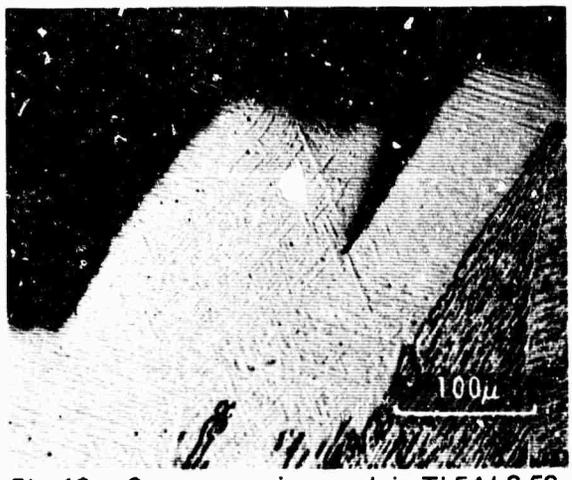

Fig. 10. Stress corrosion crack in Ti-5Al-2.5Sn martensite (2000 F/WQ).

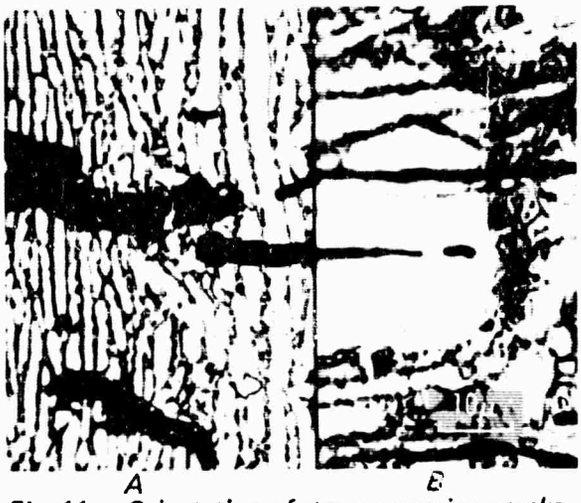

Fig. 11. Orientation of stress corrosion cracks in α stringers of Ti-8Al-1Mo-1V. Two-surface metallography, A normal to B.

in Fig. 2a) of the stringers. This is consistent with a pole figure determination (see Fig. 16) in which the (0001) planes were preferentially oriented normal to the plate surface and parallel to the rolling direction. The (0001) planes thus correspond approximately to the observed fracture planes.

Meyn (9) directly measured the orientation of the fracture planes in Ti-7Al-2Nb-1Ta by X-ray analysis, using a standard Laue back-reflection technique. He found two planes 6° from each other, both at 16° from the (0001). Hockman and Starke (Georgia Institute of Technology, private communication) also measured approximately 15° between the fracture planes and the (0001) for Ti-7Al-2Nb-1Ta. More recently, Blackburn (10) found a similar angle in Ti-8Al, where he identified the fracture plane as the $\{10\bar{1}7\}$ or $\{10\bar{1}8\}$. Thus the evidence is conclusive that cracking occurs near the basal planes.

To determine whether stress corrosion cracking could occur on other planes if the (0001) planes were not oriented favorably for crack propagation, two other specimen orientations of the same Ti-8Al-1Mo-1V material were tested in addition to the transverse-longitudinal. As shown in Fig. 12, one set of specimens was oriented with the plane of the notch and fatigue crack normal to the (0001) planes of the stringers and with the direction of main crack propagation parallel to these planes (short transverse-longitudinal). The other set was oriented with both the fatigue crack plane and main crack propagation direction normal to the (0001) planes (longitudinal-transverse). The short transverse-longitudinal specimens were made from 0.5-in.-thick plate by electron-beam-welding ends onto the plate surfaces.

Cracking in the short transverse-longitudinal specimens occurred on the same planes as in the transverse-longitudinal specimens, i.e. normal to the stringers, even though these planes were unfavorably oriented. This is shown in Fig. 13 where, to produce a continuous main crack, failure occurred in a ductile manner between the vertically cracked stringers. In the

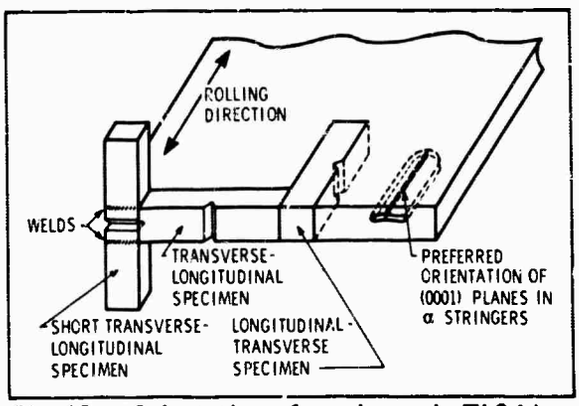

Fig. 12. Orientation of specimens in Ti-8Al-1Mo-1V 0.5-in. plate.

a. Fracture profile.

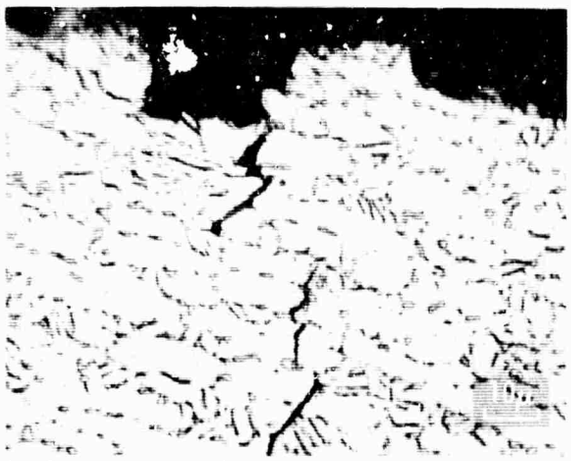

b. Secondary cracks.

Fig. 13. Cracking in short transverse specimens of Ti-8Al-1Mo-1V, viewed parallel to fracture face and to propagation direction.

longitudinal-transverse specimens, cracking again took place on the same planes, here normal to the main crack direction. Thus in this case the test results showed only slight susceptibility. Figure 14 shows the decrease in susceptibility as the fracture plane becomes less favorably oriented for crack propagation. The energy required for fracture near the basal planes is thus shown to be much less than is required on any other planes. In fact, as the upper curve indicates, the energy required for cracking on a plane other than near the basal must be roughly equal to or above that required for ductile failure in air.

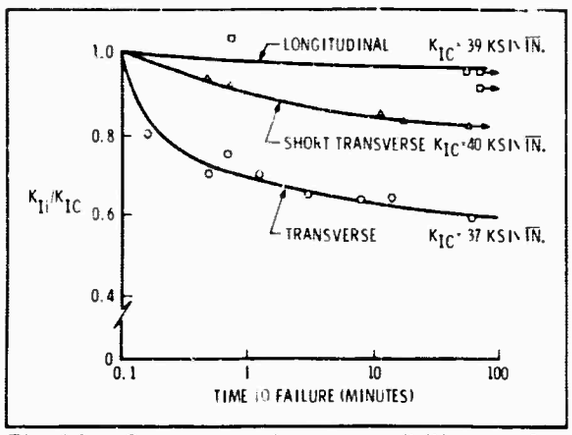

Fig. 14. Stress corrosion susceptibility as a function of specimen orientation in Ti-8Al-1Mo-1V 0.5-in. annealed plate (three-point-loaded notched bend specimens).

The microstructure of the Ti-6Al-4V 0.5-in. material had areas with equiaxed α grains which were not seen in the Ti-8Al-1Mo-1V, and had fewer stringer areas than the Ti-8Al-1Mo-1V. Cracking occurred normal to the stringers as in Ti-8Al-1Mo-1V (Fig. 15a) and was relatively continuous, inhibited only by the β phase. In contrast, cracking in the equiaxed α grains was more nearly parallel to the plate surface (i.e. more normal to the fracture face; Fig. 15b) and was thus oriented less favorably for crack propagation. Cracking in these areas was not continuous. The cracks frequently changed direction at the grain boundaries.

This difference in grain morphology and crack orientation is consistent with the difference between the pole figures for the Ti-6Al-4V and Ti-8Al-1Mo-1V 0.5-in materials. A double texture was observed in the Ti-6Al-4V: the (0001) planes were preferentially oriented either within 40° or at 90° to the plate surface, compared with 90° for the Ti-8Al-1Mo-1V (Fig. 16). [The central Ti-6Al-4V texture was rotated 90° about its center in relation to the textures normally reported for sheet material (11).] The variation in microstructure and associated texture can account for the difference in stress corrosion susceptibility between the Ti-6Al-4V and Ti-8Al-1Mo-1V (Fig. 17). Examination of other sheets and heats of Ti-8Al-1Mo-1V and Ti-6Al-4V has shown a large variation in micro-

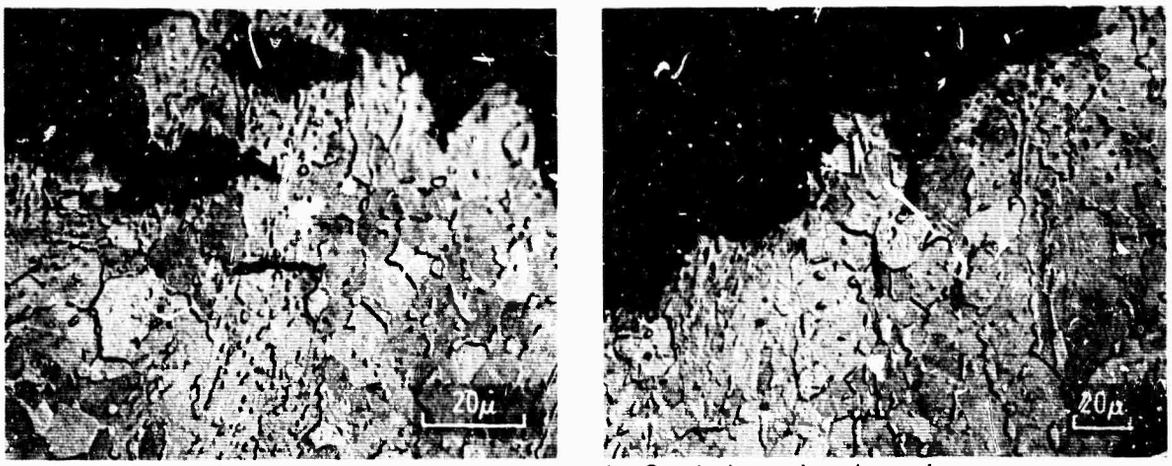

a. Cracks in α stringer areas. *b. Cracks in equiaxed α grains.*

Fig. 15. Stress corrosion cracking in annealed Ti-6Al-4V 0.5-in. plate, viewed parallel to propagation direction.

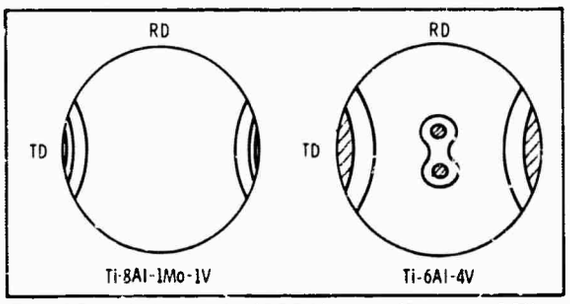

Fig. 16. Schematic (0001) pole figures of Ti-8Al-1Mo-1V and Ti-6Al-4V 0.5-in. annealed plate.

structure due to differences in processing. Thus the same or wider variations in susceptibility can be expected to occur in a single alloy.

It is well established that there is a thickness effect on the stress corrosion behavior of high-α alloys (4, 12, 13). Less susceptibility is normally obtained for thinner-gage material (Fig. 18); with a thin enough gage, immunity can be obtained. In an attempt to eliminate microstructural differences as the cause, Wald (12) conducted stress corrosion tests on Ti-6Al-4V and Ti-8Al-1Mo-1V plate material,

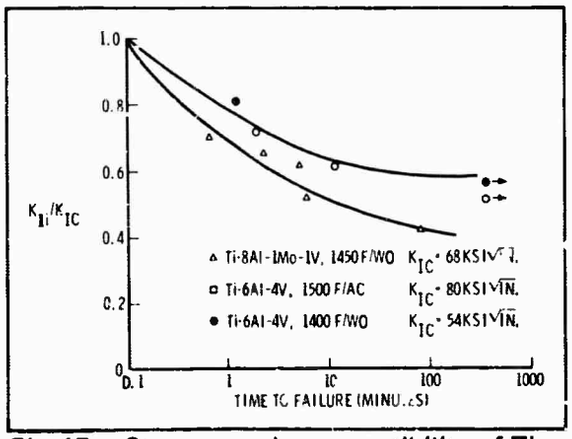

Fig. 17. Stress corrosion susceptibility of Ti-8Al-1Mo-1V and Ti-6Al-4V 0.5-in. annealed plate (large four-point-loaded notched bend specimens).

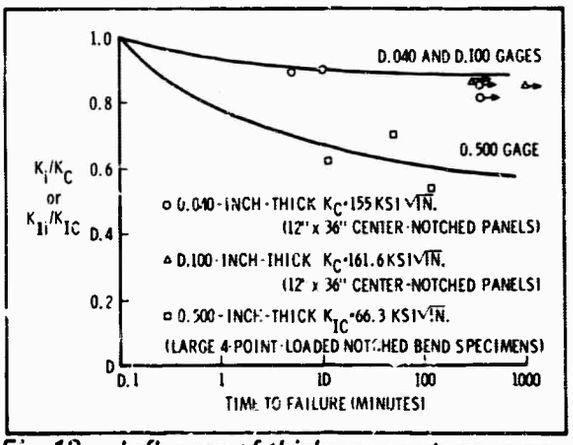

Fig. 18. Influence of thickness on stress corrosion susceptibility of annealed Ti-6Al-4V.

machined this same material to thinner dimensions, and retested. The thinner specimens were less susceptible, demonstrating that the thickness effect is largely due to the state of stress. The change from thin- to thick-gage material corresponds to a change from a biaxial to a triaxial stress state (notched specimens).

The influence of stress state can be partly explained by the fact that cracking in the α phase must occur near the single (0001) plane. For example, during the stress corrosion process, only those grains that have these fracture planes oriented to allow a sufficient normal stress component for cracking will fail by stress corrosion. The others will fail in a ductile manner. In a stress corrosion test with a biaxial stress state, more grains are oriented for fracture than with a uniaxial stress state. It follows that the triaxial stress state would have the most grains oriented for fracture and should show the highest susceptibility to stress corrosion.

In addition to the stress state, preferred orientation apparently also contributes to the thickness effect. As shown in Fig. 18, relative immunity is obtained in Ti-6Al-4V at a gage thickness of 0.100 in. This is inconsistent with Wald's data (12), where 0.050 in. was the greatest thickness at which Ti-6Al-4V showed relative immunity. This can be explained by the change in preferred orientation with thickness observed in high-α alloys. Baggerly (Ref. 14 and private communication) has shown by X-ray diffraction in Ti-8Al-1Mo-1V and Ti-6Al-6V-2Sn that the (0001) planes in the 0.5-in.-thick material are oriented preferentially normal to the plate surface and parallel to the rolling direction. Examining thinner-gage material, he found that the texture changes to that usually reported (11) for titanium alloys: i.e. the (0001) planes are tilted 20° to 30° from the plane of the sheet surface. The (0001) planes are thus less favorably oriented for cracking in processed sheet gage than in plate material thinned to sheet dimensions (transverse specimens).

A comparison of the microstructures of Ti-8Al-1Mo-1V plate (Fig. 2a) versus sheet material (Fig. 19) shows that stringers are typical of plate but are much less common in the thinner gages, where equiaxed grains predominate. As in the earlier comparison between the Ti-6Al-4V and Ti-8Al-1Mo-1V 0.5-in. plate, this indicates that the equiaxed grains tend to have their (0001) planes oriented within 40° of the sheet surface.

The differences in preferred orientation and grain morphology between sheet and plate material are believed to be due to differences in rolling temperature and amount of reduction. The α phase transformed from the β via the Burgers relationship $\{110\}\ \langle 111\rangle_\beta \parallel (0001)\ \langle 11\bar{2}0\rangle_\alpha$ will have the texture found in 0.5-in. plate if the β phase (during β rolling) assumes the typical bcc rolling texture (001) [110] and if the rolling stresses cause one variant of the transformation to be preferred (14). After the initial β rolling, the thicker gages are rolled at temperatures in the $\alpha+\beta$ region that are apparently high enough so that α recrystallization does not occur and the stringer structure results. Thinner gages are reduced more and are rolled at lower temperatures so that the deformed structure apparently has enough stored energy for α recrystallization to occur with subsequent annealing. This deformation and recrystallization process apparently produces the equiaxed grains typical of sheet material.

It seems likely that drastic differences in stress corrosion susceptibility could be obtained with different combinations of stress state and preferred orientation. In a biaxial-stress-state test, for instance, little cracking should occur when the preferred orientation is such that most of the fracture planes are normal to the axis in which the stress is zero. When, instead, most of

Fig. 19. Microstructure of Ti-8Al-1Mo-1V 0.010-in. annealed sheet, longitudinal view.

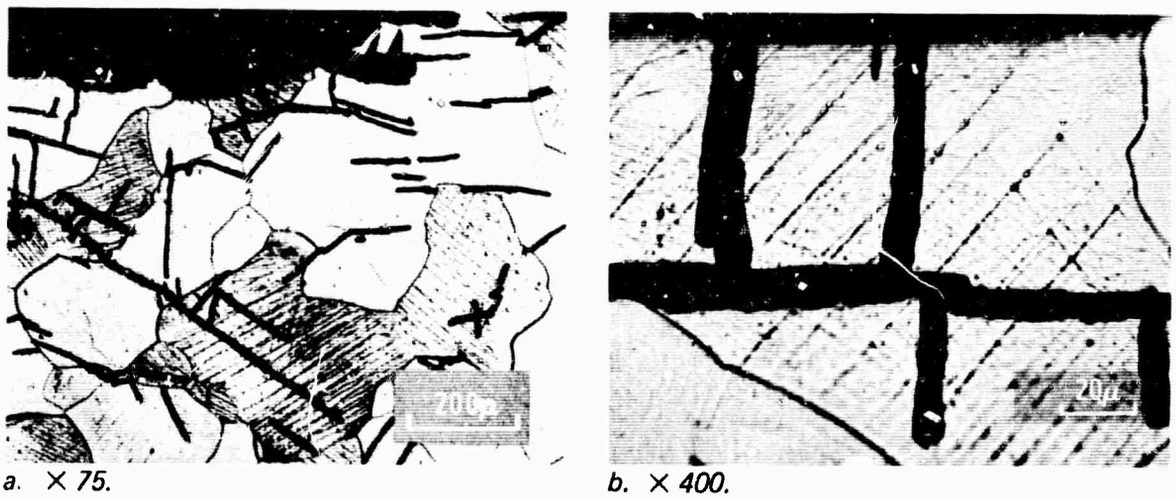

a. × 75. b. × 400.

Fig. 20. Stress corrosion cracking in the β phase of solution-treated Ti-13V-11Cr-3Al (1575 F/WQ).

the fracture planes are oriented normal to the major stress axis, cracking should be extensive.

CRACKING CHARACTERISTICS IN THE BETA PHASE

Stress corrosion cracks in the β phase of Ti-13V-11Cr-3Al are crystallographic (Fig. 20). Cracks commonly occur on two or sometimes three different crystallographic planes in a single grain. This is in contrast to the single-plane cracking normally observed in the α phase of the high-α alloys. Figure 21 demonstrates the brittle fracture mode in the β phase; note the grain boundary extending through A and B and the numerous parallel crack branches connected by ductile tearing.

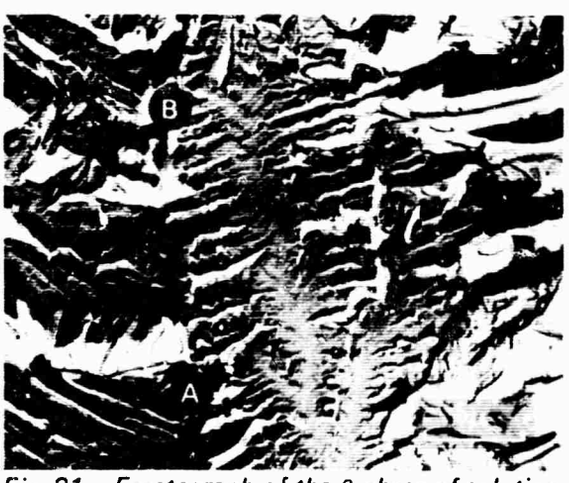

Fig. 21. Fractograph of the β phase of solution-treated Ti-13V-11Cr-3Al (1575 F/WQ). Grain boundary extends through A and B.

A lactic-acid etch was used to reveal the slip lines in the deformed grains of this alloy (Fig. 20). Many of the lines were composed of individual dislocation etch pits. An analysis of the relation between the cracks and slip lines in one surface showed that in about 60% of the cases where two or more different slip systems were observed in a single grain, the cracks roughly bisected them. This, together with the assumption that slip occurs mainly on the $\{110\}$ planes, indicates that cracking occurs on the $\{100\}$ planes. Crack branching in single grains was extensive, yet no more than three fracture-plane orientations were observed by use of one-surface and two-surface metallography. This tends to eliminate all planes except the $\{100\}$ and (possibly) the $\{111\}$.

Two-surface trace analyses on a number of grains revealed angles of approximately 80° or 90° between cracks (predominantly 80°):

Grain	Angle between fracture planes (accuracy < ±5°)
1	90°
2	91°
3	84°
4	79°
5	80°
6	79°
7	80°
8	78°

The 80° measurements are inconsistent with cracking on the $\{100\}$ planes and appear to be outside the limit of error of the analyses. It is remotely possible that the cracking occurs on the $\{210\}$ planes instead of the $\{100\}$ (15). If this is true, however, it remains to be explained why only the planes with the higher angles between them crack, and why no more than three out of a possible 24 planes crack in a single grain. The 80° and 90° measurements can be explained by an irrational plane near the $\{100\}$ which, considering the fracture plane in α, may not be unrealistic. At present it is reasonable to conclude that cracking occurs on or near the $\{100\}$ planes.[3]

Cracking in the β phase of this alloy is inhibited to some extent when the α phase is present as the result of an aging treatment (Fig. 22). As shown, the cracks take irregular paths through the β grains. (Note in Fig. 22 that slip lines are no longer observed after etching.) The crack inhibition by the α does not necessarily mean that this phase is immune in this alloy. Assuming that cracks occur on the $\{100\}$ planes in the β and on the (0001) in the α, crack inhibition would be expected from the Burgers relationship $\{110\}_\beta \parallel (0001)_\alpha$. A fractographic analysis to determine whether the α precipitate failed by stress corrosion was inconclusive.

There appear to be two microstructural features inhibiting crack propagation in Ti-13V-11Cr-3Al: (1) the grain boundaries in both the solution-treated and solution-treated-plus-aged conditions, and (2) the α precipitate in the aged conditions. Their direct effect could not be determined because of an overriding influence of toughness on measured susceptibilities. However, the toughness was a function of the variations in these features; thus they influenced susceptibility indirectly.

By testing thin notched bend specimens (0.125 in.), susceptibility to stress corrosion was found to be proportional to the "apparent fracture toughness" (see Experimental Procedure section) of the heat-treatment condition (Table II). Microscopic examination of the specimens showed that cracks had initiated on the surfaces in the plastic yield zones, independent of the main crack. This effect produced the unusual crack tip shape shown schematically in Fig. 23.

The size of the plastic yield zone increases as K_{IC} increases and as σ_{YS} decreases, by the formula

$$R = \frac{1}{2\pi}\left(\frac{K_{IC}}{\sigma_{YS}}\right)^2$$

where R is the radius of the plastic yield zone and σ_{YS} is the yield strength (16). The surface yielding and resultant surface cracking would thus be more extensive in heat-treatment conditions of higher toughness and lower yield strength, as was observed. This influence of toughness on susceptibility would not be expected with a valid specimen configuration (5), but was included here to point out a major difference between a susceptible β and a susceptible α alloy.

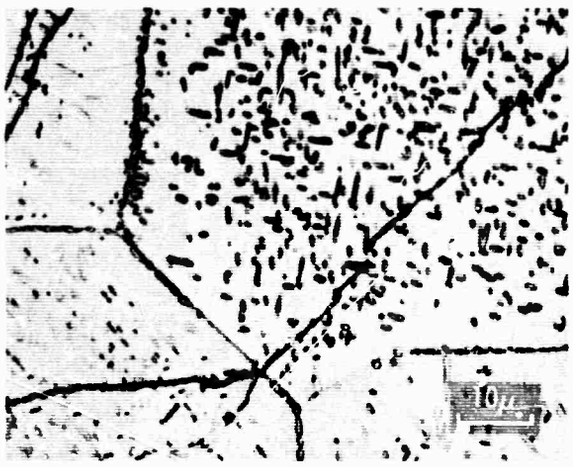

Fig. 22. Effect of α precipitate on crack propagation of solution-treated-plus-aged Ti-13V-11Cr-3Al (1725 F/WQ + 1200 F/WQ).

[3]This was confirmed just prior to publication. Using the back-reflection Laue technique, the fracture plane in a large grain was found to be within 7° of the $\{100\}$.

Table II. Variation in stress corrosion susceptibility with "apparent fracture toughness" for Ti-13V-11Cr-3Al.

(3-point-loaded notched bend specimens, 0.125 in. thick)

Heat-treat condition	"Apparent fracture toughness" (ksi $\sqrt{in.}$) (a)	Stress corrosion susceptibility (b)
1725 F/15 min/WQ + 1200 F/24 hr/WQ	37	0.85
1450 F/15 min/WQ + 875 F/30 min/AC	54	0.75
1450 F/15 min/AC	78	0.50
1725 F/15 min/WQ	87	0.40
1575 F/1 hr/WQ	89	0.30

[a] As these values increase, the corresponding yield strengths decrease.

[b] Ratio of the minimum of the sustained-load curve in salt solution to the "apparent fracture toughness."

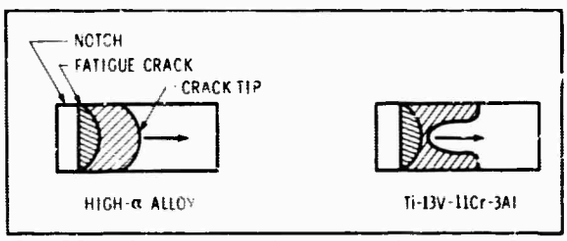

Fig. 23. Stress corrosion crack-tip shapes for Ti-13V-11Cr-3Al and typical high-α alloy.

There are two major differences in behavior between the susceptible α phase of the high-α alloys and the β phase of Ti-13V-11Cr-3Al. First, as thinner material is tested, surface yielding increases because of the increase in plastic yield zone relative to material thickness. In the α alloys, as shown previously, susceptibility decreases as thickness decreases. This is opposite to the behavior shown above for the β alloy. Second, unnotched tensile specimens of the β alloy fail prematurely in salt solution; in all such tests run during this study, failure occurred below the 0.2% yield limit. Similar failures in the α alloy are either impossible or require special conditions; tests run with the average (0001) planes normal to the stress axis were unsuccessful.

These differences in behavior in which the β is more susceptible to stress corrosion, at least in the uniaxial stress state, are difficult to explain. One possibility is the presence of both a normal stress criterion and a slip criterion for cleavage, as in the fracture of zinc (17, 18, 19). The criteria might be easily satisfied by the bcc' β phase in the uniaxial stress state. In the lower-symmetry hexagonal α, however, a biaxial stress state might be necessary because of the relationship between the fracture plane and the required slip system.

MECHANISM

The basic stress corrosion mechanism is generally considered to involve an interaction beween a surface process (e.g. an electrochemical reaction) and a structural or mechanical failure process. Assuming that the two processes may be treated independently, one or possibly both is

rate-controlling and therefore can be influenced by a variable such as heat treatment. One problem then in defining the basic mechanism is to determine whether it is surface-controlled or structurally controlled, or both.

Structural characteristics vary considerably among the three susceptible phases α in Ti-8Al-1Mo-1V, martensite in Ti-5Al-2.5Sn, and β in Ti-13V-11Cr-3Al. In the α phase (ordered or disordered), slip occurs on the (0001), $(10\bar{1}1)$, and $(10\bar{1}0)$ planes, mainly on the $(10\bar{1}0)$. Dislocations tend to lie in coplanar groups in preference to a cellular arrangement (8). This phase is relatively ductile, exhibiting about 15% elongation.

The hexagonal martensite of Ti-5Al-2.5Sn has a typical acicular structure with internal stacking faults (Fig. 24). Coplanar dislocations are found in some grains upon deformation at room temperature, indicating a tendency toward coplanar arrays rather than tangles if the orientation is suitable. This phase has the low ductility (about 8% elongation) typical of the titanium martensites. Many areas of its structure show only one variant of the martensitic transformation (see Fig. 10), compared with a minimum of three always observed in Ti-8Al-1Mo-1V. This is evidently a function of the cooling rate: in thinner material quenched from 2000°F, these areas are much reduced. Otherwise, the structure and deformation characteristics of this phase are similar to those of α'' in Ti-8Al-1Mo-1V.

The β phase of Ti-13V-11Cr-3Al has an extremely large grain size in comparison to those of the high-α alloys. Its high ductility (about 20% elongation) is apparently due to extensive slip and twinning. (X-ray analysis showed no sign of strain-induced martensite in a highly strained specimen.) A limited attempt to determine the dislocation configuration by transmission electron microscopy was unsuccessful, although the coarse slip line structure observed by optical microscopy indicates a coplanar configuration.

The structures of the nonsusceptible phases α', α'', and β in Ti-8Al-1Mo-1V and martensite in Ti-6Al-4V also vary considerably. The α' phase has a crystal structure tentatively identified as fcc, with an internally-twinned-acicular morphology (7). The hexagonal α'' has a larger acicular structure with internal stacking faults

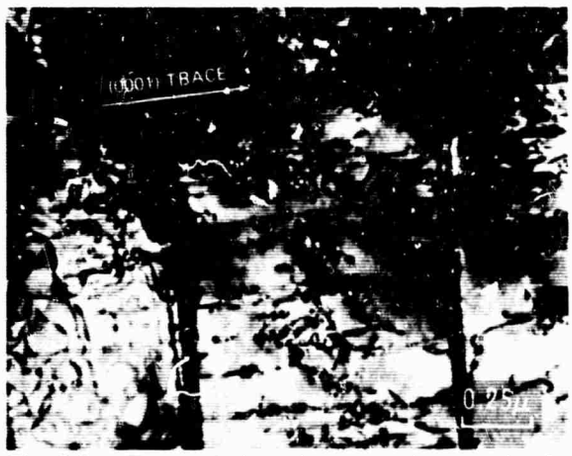

Fig. 24. Transmission electron micrograph of Ti-5Al-2.5Sn martensite (2000 F/WQ).

(7). Both the α' and the α'' have grains that contain severe dislocation tangling. The internal structures of these two phases would be expected to limit slip; this is confirmed in α'', which exhibits low ductility (about 5% elongation). The dislocations formed in α'' by room-temperature deformation can be found to lie in coplanar arrays (Fig. 25). The β phase of Ti-8Al-1Mo-1V has an extremely small grain size. Because of its high molybdenum and vanadium content, this phase would be expected to have high ductility, similar to the β phase of Ti-13V-11Cr-3Al (11). The martensite of Ti-6Al-4V has been shown to be similar to the α'' of Ti-8Al-1Mo-1V (20).

The only common structural feature among either the susceptible or nonsusceptible phases that can control susceptibility appears to be the presence of coplanar dislocation arrays. A number of stress corrosion mechanisms have been suggested that are based on the necessity for a coplanar, rather than cellular, dislocation configuration. However, the presence of coplanar dislocation arrays in the immune phase α'' of Ti-8Al-1Mo-1V indicates that although this configuration may be necessary, it does not control susceptibility. It has been proposed for other alloy systems (21) that coplanar dislocations may be necessary but not sufficient for stress corrosion cracking. In this regard, it is possible that the grain size of the three immune phases α', α'', and β in Ti-8Al-1Mo-1V is small enough so that dislocation pileups cannot produce high enough stresses for fracture

Fig. 25. Transmission electron micrograph of dislocation structure after ~2% plastic strain in the α″ phase of Ti-8Al-1Mo-1V.

[e.g. via Stroh's fracture mechanism (22)]. This does not appear reasonable, however, because when the immune α″ was aged, the structure became susceptible without any change in grain size (Fig. 7).

Because it predicts cracking on the {100} planes, the Cottrell locking mechanism (23) has been considered as an explanation for cracking in Ti-13V-11Cr-3Al. However, cracking occurred at stresses near the proportional limit in tensile tests on unnotched specimens. It seems unlikely that such a stress level would be high enough to create dislocation pileups that could initiate cracks by this mechanism.

In view of the fact that the three immune phases of Ti-8Al-1Mo-1V (α′, α″, and β) all have a high Mo and V content (β stabilizers) and low Al and O content (α stabilizers) relative to the susceptible α phase, yet show considerable variation in structure, it appears that the basic mechanism is surface-controlled rather than structurally controlled.

Conclusions

1. The α phase is susceptible, whereas the β and martensite phases are immune to stress corrosion in the Ti-8Al-1Mo-1V, Ti-6Al-4V, and Ti-4Al-3Mo-1V alloys. Stress corrosion susceptibility thus decreases as the percentage of either of these latter two phases increases.

2. In the α phase, stress corrosion cracks generally can occur only near the (0001) plane. This results in an influence of preferred orientation and state of stress on the stress corrosion susceptibility of high-α alloys.

3. Stress corrosion cracks occur on or near the {100} planes in the β phase of Ti-13V-11Cr-3Al.

4. In uniaxial and possibly in biaxial stress states, stress corrosion effects are more severe in a susceptible β phase than in a susceptible α phase.

5. The basic mechanism is apparently surface-controlled, since susceptibility could be correlated with phase chemistry but not with phase structure.

Acknowledgments

The authors wish to thank the many persons who contributed to this work: in particular, D. A. Rothfuss and W. D. Swift for performing most of the stress corrosion tests, R. J. LaPorte and S. R. Mitchell for the optical metallography, R. G. Baggerly and W. E. Quist for helpful advice and discussions, and Dr. D. E. Piper for reviewing and helping to prepare the manuscript.

This research was supported by the Advanced Research Projects Agency of the Department of Defense (ARPA Order 878) and was monitored by the Naval Research Laboratory under Contract No. N00014-66-C0365.

References

1. B. F. Brown, A New Stress-Corrosion Cracking Test for High-Strength Alloys, Materials Research and Standards, 6, No. 3 (1966), p 129.

2. F. A. Crossley, C. J. Reichel, and C. R. Simcoe, The Determination of the Effects of Elevated Temperatures on the Stress Corrosion Behavior of Structural Materials, Armour Research Foundation of Illinois Institute of Technology, WADD Tech Report 60-191 (May 1960).

3. J. G. Hines, On the Propagation of Stress Corrosion Cracks in Metals, Corrosion Sci, 1 (1961), p 21.

4. D. E. Piper, S. H. Smith, and R. V. Carter, Corrosion Fatigue and Stress-Corrosion Cracking in Aqueous Environments, to be published in Metals Engineering Quarterly.

5. J. E. Srawley and W. F. Brown, Fracture Toughness Testing Methods, Fracture Toughness Testing and Its Applications, ASTM STP 381 (1965), p 133.

6. I. R. Lane, Jr., J. L. Cavallaro, and A. G. S. Morton, Sea Water Embrittlement of Titanium, Stress-Corrosion Cracking of Titanium, ASTM STP 397 (1966), p 246.

7. M. J. Blackburn, Phase Transformations in the Alloy Ti-8Al-1Mo-1V, ASM Trans. 59, No. 4 (1966), p 876.

8. M. J. Blackburn, Relationship of Microstructure to Some Mechanical Properties of Ti-8Al-1Mo-1V, ibid, p 694.

9. D. A. Meyn, A Study of the Crystallographic Orientation of Cleavage Facets Produced by Stress-Corrosion Cracking of Ti-7Al-2Nb-1Ta in Water, Report of NRL Progress (August 1965).

10. T. R. Beck and M. J. Blackburn, Stress Corrosion Cracking of Titanium Alloys: Electrochemical Mass-Transport-Kinetic Model, Metallurgical and Mechanical Effects, and Proposed Relation of Electrochemical, Metallurgical and Mechanical Effects, Boeing Scientific Research Laboratories Document NAS 7-489 (June 1967).

11. R. I. Jaffee, The Physical Metallurgy of Titanium Alloys, Progress in Metal Physics, 7 (1958).

12. G. G. Wald, Effect of Heat Treatment on Salt Water Delayed Fracture of Titanium Alloys, paper presented at the 96th AIME Annual Meeting, Los Angeles, California (1967).

13. N. G. Feige and T. Murphy, Fracture Behavior of Titanium Alloys in Aqueous Environment, Metals Engineering Quarterly, 7, No. 1 (February 1967), p 53.

14. R. G. Baggerly, Determination of Preferred Orientation with the Norelco Pole Figure Device, Boeing Document D1-36002-1 (1964).

15. C. S. Barrett, Structure of Metals, McGraw-Hill, New York (1952), 2nd ed., p 36.

16. Fracture Testing of High Strength Sheet Materials, First Report of Special ASTM Committee, ASTM Bulletin (January 1960).

17. A. Deruyttere and G. B. Greenough, The Criterion for the Cleavage Fracture of Zinc Single Crystals, J Inst Metals, 84 (1956), p 337.

18. J. J. Gilman, Fracture of Zinc-Monocrystals and Bicrystals, Trans AIME, 212 (1958), p 783.

19. M. H. Kamdar and A. R. C. Westwood, Embrittlement of Zinc Monocrystals and Bicrystals by Mercury and Gallium, Environment-Sensitive Mechanical Behavior, A. R. C. Westwood and N. S. Stoloff, eds., Gordon and Breach, New York (1966).

20. J.C. Williams and M. J. Blackburn, A Comparison of Phase Transformations in Three Commercial Titanium Alloys, to be published in ASM Trans (September 1967).

21. P. R. Swann and J. D. Embury, Microstructural Aspects of Stress-Corrosion Failure, High-Strength Materials, V. F. Zackay, ed., J. Wiley & Sons, New York (1965).

22. A. N. Stroh, A Theory of the Fracture of Metals, Advances in Physics, 6 (1956-57), p 418.

23. A. H. Cottrell, Theory of Brittle Fracture in Steel and Similar Metals, Trans AIME, 212 (April 1958), p 192.

14 KEY WORDS	LINK A ROLE	LINK A WT	LINK B ROLE	LINK B WT	LINK C ROLE	LINK C WT
Titanium Alloys						
Aqueous Stress Corrosion Susceptibility						
Preferred Grain Orientation						
Immune Phase						
State of Stress						
Grain Morphology						
Thickness Effect						
Crack Inhibition						

Unclassified

Security Classification

DOCUMENT CONTROL DATA - R & D

(Security classification of title, body of abstract and indexing annotation must be entered when the overall report is classified)

1. ORIGINATING ACTIVITY *(Corporate author)*

The Boeing Company
Commercial Airplane Division
Renton, Washington

2a. REPORT SECURITY CLASSIFICATION

2b. GROUP

3. REPORT TITLE

Some Characteristics of Aqueous Stress Corrosion in Titanium Alloys

4. DESCRIPTIVE NOTES *(Type of report and inclusive dates)*

Research Report

5. AUTHOR(S) *(First name, middle initial, last name)*

Daniel N. Fager
William F. Spurr

6. REPORT DATE

September 1967

7a. TOTAL NO. OF PAGES

17

7b. NO. OF REFS

23

8a. CONTRACT OR GRANT NO.

N00014-66-C0365

b. PROJECT NO.

c.

d.

9a. ORIGINATOR'S REPORT NUMBER(S)

9b. OTHER REPORT NO(S) *(Any other numbers that may be assigned this report)*

Boeing Document D6-60083

10. DISTRIBUTION STATEMENT

Reproduction in whole or in part is permitted by the United States Government. Distribution of this document is unlimited.

11. SUPPLEMENTARY NOTES

12. SPONSORING MILITARY ACTIVITY

Advanced Research Projects Agency, Department of Defense

13. ABSTRACT

The influence of microstructural features on the stress corrosion fracture path has been studied in the alloys Ti-8Al-1Mo-1V, Ti-6Al-4V, Ti-4Al-3Mo-1V, Ti-5Al-2.5Sn, and Ti-13V-11Cr-3Al by means of optical microscopy, electron microscopy, and X-ray diffraction. These studies have shown that susceptibility of titanium alloys to aqueous stress corrosion is influenced by crystalline structure of the susceptible phase (bcc or hcp), preferred grain orientation, and relative phase content where one phase is immune. Stress corrosion cracking occurs on or near the (100) planes in the bcc beta phase, but can only occur near the single (0001) plane in the hcp alpha phase. This restriction of cracking in the alpha phase results in a significant influence due to preferred orientation; it also contributes to the influence of stress state on susceptibility in the high-alpha alloys. The apparent lack of correlation between the structures of the phases and their stress corrosion susceptibilities indicates that the basic mechanism is surface-controlled rather than structurally controlled.

DD FORM 1 NOV 65 1473

Unclassified

Security Classification